International Journal of Biological Macromolecules 239 (2023) 124328

Contents lists available at ScienceDirect

International Journal of Biological Macromolecules

journal homepage: www.elsevier.com/locate/ijbiomac

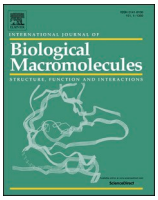

Cellulose based polyurethane with amino acid functionality: Design, synthesis, computational study and application in wastewater purification

Haneen Abu Rub [a], Abdalhadi Deghles [b,*], Othman Hamed [a,*], Khalil Azzaoui [c,*], Belkheir Hammouti [d], Mustapha Taleb [c], Avni Berisha [e,f], Omar Dagdag [g,h], Waseem Mansour [a], Gül Gülenay Hacıosmanoğlu [i], Zehra Semra Can [i], Larbi Rhazi [j,*]

[a] Chemistry Department, Faculty of Science, An-Najah National University, P.O. Box 7, Nablus, Palestine
[b] Istiqlal University, Jericho, Palestine
[c] Laboratory of Engineering, Electrochemistry, Modeling and Environment, Faculty of Sciences, Sidi Mohamed Ben Abdellah University, B.P. 1796, Fez, Morocco
[d] Laboratory of Applied Chemistry and Environment LCAE, Faculty of Sciences, First Mohammed University, P.O. Box 717, Oujda 60 000, Morocco
[e] Department of Chemistry, Faculty of Natural and Mathematics Science, University of Prishtina, Prishtina 10000, Kosovo
[f] Materials Science-Nanochemistry Research Group, NanoAlb-Unit of Albanian Nanoscience and Nanotechnology, Tirana 1000, Albania
[g] Laboratory of Mineral Solid and Analytical Chemistry LMSAC, Department of Chemistry, Faculty of Sciences, Mohamed 1St University, P.O. Box 717, Oujda, Morocco
[h] Centre for Materials Science, College of Science, Engineering and Technology, University of South Africa, Johannesburg, South Africa
[i] Marmara University, Environmental Engineering Department, Istanbul, Turkey
[j] Institut Polytechnique UniLaSalle, Université d'Artois, ULR 7519, 19 rue Pierre Waguet, BP 30313, 60026 Beauvais, France

ARTICLE INFO

Keywords:
Foam
Cellulose
Olive waste biomass
Wastewater
Toxic metal ions

ABSTRACT

Contamination in water is due to various environmental pollutants from natural and anthropogen activities. To remove toxic metals from contaminated water, we developed a novel adsorbent in foam form based on an olive industry waste material. The foam synthesis involved oxidation of cellulose extracted from the waste to dialdehyde, functionalization of the cellulose dialdehyde with an amino acid group, reacting the functionalized cellulose with hexamethylene diisocyanate and *p*-phenylene diisocyanate to produce the target polyurethanes Cell-F-HMDIC and Cell-F-PDIC, respectively. The optimum condition for lead(II) adsorption by Cell-F-HMDIC and Cell-F-PDIC were determined. The foams show the ability to quantitatively remove most of metal ions present in a real sample of sewage. The kinetic and thermodynamic studies confirmed a spontaneous metal ion binding to the foams with a second pseudo-order adsorption rate. The adsorption study revealed it obeys the Langmuir isotherm model. The experimental Qe values of both foams Cell-F-PDIC and Cell-F-HMDIC were 2.1929 and 2.0345 mg/g, respectively. Monte Carlo (MC) and Dynamic (MD) and simulations showed excellent affinity of both foams for lead ions with high adsorption negative energy value indicating vigorous interactions of Pb(II) with the adsorbent surface. The results indicate the usefulness of the developed foam in commercial applications.

Environmental implication: Elimination of metal ions from contaminated environments is important for a number of reasons. They are toxic to humans via interaction with biomolecules, resulting in disruption of the metabolism and biological activities of many proteins. They are toxic to plants. Industrial effluents and/or wastewater discharged from production processes, contain a considerable amount of metal ions.

In this work, the use of naturally produced materials, such as olive waste biomass, as adsorbents for environmental remediation has received great attention. This biomass represents unused resources and presents serious disposal problems. We demonstrated that such materials are capable of selectively adsorbing metal ions.

1. Introduction

Water contamination is becoming a major global concern as agricultural waste, industrial waste, and the household washing items are disposed in the sewage system [1]. The disposed materials are known to release toxic materials include organic matters, metal ions,

* Corresponding authors.
E-mail addresses: daghlas2014@pass.ps (A. Deghles), ohamed@najah.edu (O. Hamed), k.azzaoui@yahoo.com (K. Azzaoui), larbi.rhazi@unilasalle.fr (L. Rhazi).

https://doi.org/10.1016/j.ijbiomac.2023.124328
Received 18 February 2023; Received in revised form 27 March 2023; Accepted 31 March 2023
Available online 3 April 2023

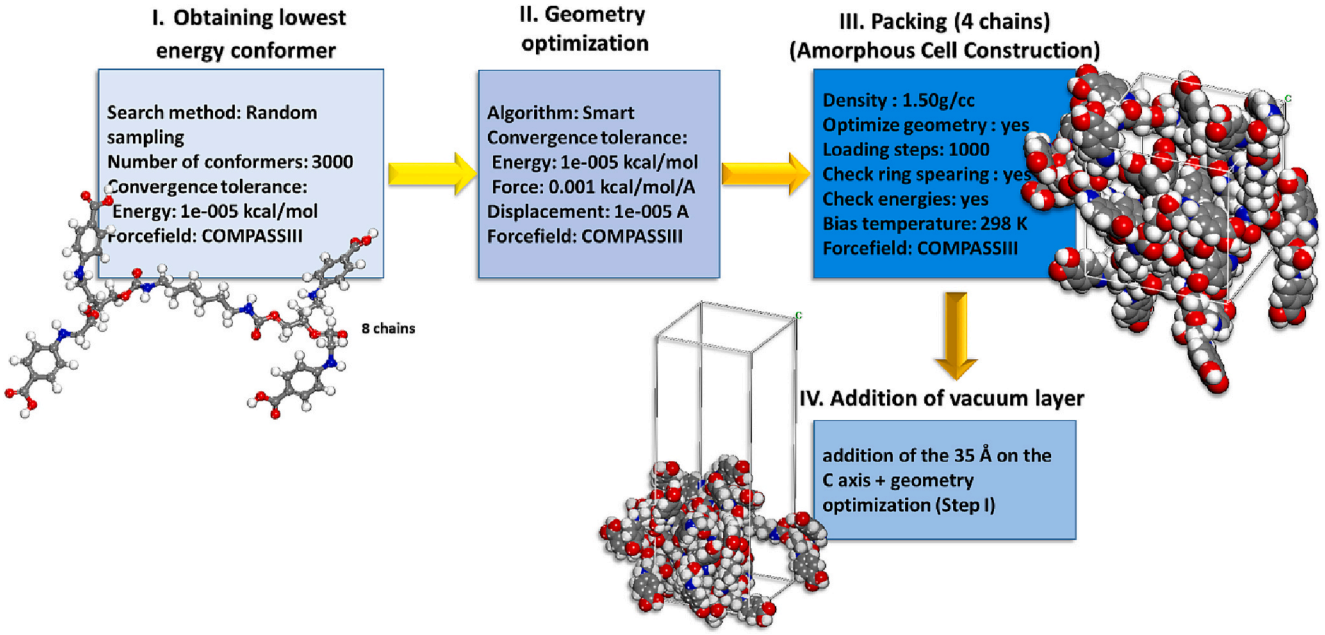

Fig. 1. The steps and accompanying calculation details for building the Cell-F ascorbates PBC model.

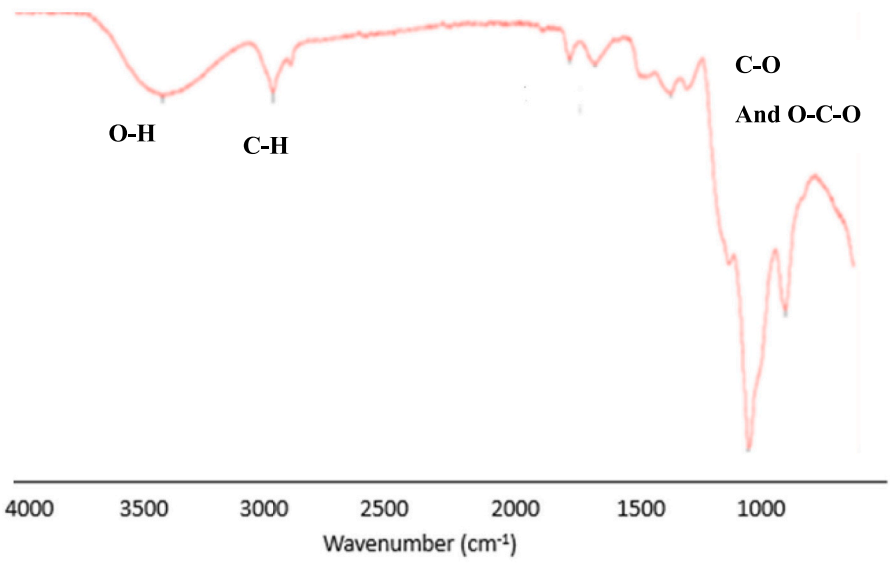

Fig. 2. FT-IR spectrum of Cell-DA.

dyes and others [2–4]. Toxic heavy metal ions such as Mn(II), Cd(II), Co (II), Ni(II), Cr(III), Zn(II), Cu(II), Pb(II) and others pose a high health risk and need immediate attention [5,6]. Wastewater purification by adsorption is one of the most effective and least cost technology used for making water reusable for purposes other than drinking [7]. Adsorption is a simple, convenient method, and can be run at low cost. Many adsorbents are available for use in this technology that are ecofriendly, recyclable, and safe [8–10]. Ecofriendly adsorbents such as those made from cellulose, lignin, and chitosan [11–14] showed high efficacy for toxic heavy metal ions present in wastewater [15]. Despite the rapid enhancement in the development of adsorbents, those originated from natural macromolecules such as those made from cellulose, microcrystalline cellulose or nanocellulose have not been fully explored [16–20]. Adsorbents made from cellulose nanocrystalline (CNC) were among the most promising, however, they suffer from several drawbacks that are related to crystallinity which limits the accessibility to backbones binding sites [21,22].

A convenient solution for this issue was done by impeding carboxymethyl cellulose in a PU foam matrix and used it as metals adsorbent [21]. The work is interesting but will not solve the accessibility and the aggregation issue in the cellulose polymer. In this study, new cellulose-based foam with ionic functionality was prepared and used as an adsorbent of metals present in wastewater. Polyurethane foam (PUF) was selected because of its attractive characteristics that include elasticity, porosity with controllable pore structure. The attractive parts of the foams are the simple process of making it, the high stability, and the high porosity which make it adsorb and desorb in a high rate. It is also easy to isolate and recycle, all these factors make foams very suitable for use as an adsorbent for wastewater purification. Recently, several research studies investigated the possibility of using PU as an adsorbent

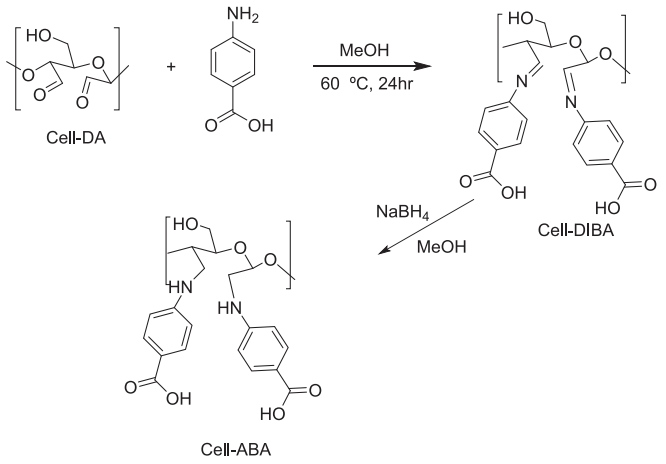

Fig. 3. Preparation of cellulose diaminobenzoic acid (Cell-ABA).

for organic matters and toxic metal ions [22,23]. Some PUF showed excellent adsorbent properties due to its resistant to change in pH value, high surface area, low cost, and high stability in aqueous and organic solvents [24]. It has been shown that, PUFs can be used in a continuous or batch process [25]. PUF with no active groups for metal ions has limited activity as an adsorbent, in additions it suffers from the low rate of adsorption and low selectivity [26]. Whereas PUF chemically of physically modified and composite showed improvement in adsorption and selectivity for organic matters and metal ions [27].

In this project the disadvantages present in PUF reported in the literature as an adsorbent for metal ions were eliminated by preparing cellulose based polyurethane foam with ionic functional groups that are covalently attached to it. Cellulose powder employed in this work was isolated from the solid waste of the olive industry (OISW) [20]. The prepared foams with multidentate chelating pendant groups showed high affinities for toxic heavy metals. The adsorption efficiencies of the two foams were evaluated toward Pb(II) and other metal ions present in sewage. Kinetic and thermodynamic analysis in addition to Monte Carlo (MC) and Dynamic (MD) and simulations were performed on the foam as adsorbent.

2. Experimental

2.1. Material

All staring materials and reagents employed in this study were of analytical grade (Sigma-Aldrich Chemical Company, Jerusalem) and used as received. The chemicals are hexamethylene diisocyanate, 1,4-pheneylne diisocyanate, sodium chloroacetate, and lead(II) nitrate. All solutions were prepared using deionized water. Cellulose used in this study was in powder form, it was isolated from the solid waste of the olive industry by the kraft cooking process that was developed by our research team [20].

2.2. Characterization

FT-IR (Fourier Transform Infrared spectrometer) analysis was performed on Nicolet 6700 by Thermo-Fisher Scientific (MA, USA) furnished with the Smart Split Pea micro-ATR accessory. The IR parameters settings were the resolution was 4 cm^{-1}, spectral range 600–4000 cm^{-1}, and number of scans 256. Thermal behavior of the prepared foam was studied using Thermo-gravimetric analysis (TGA) TG/DSC Star System (Mettler-Toledo) equipped with a HT1100 oven that is connected to a

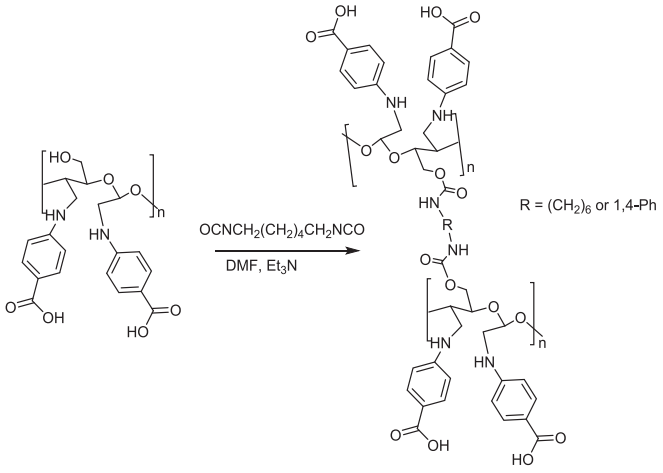

Fig. 5. A representative scheme showing the formation of polyurethane foam.

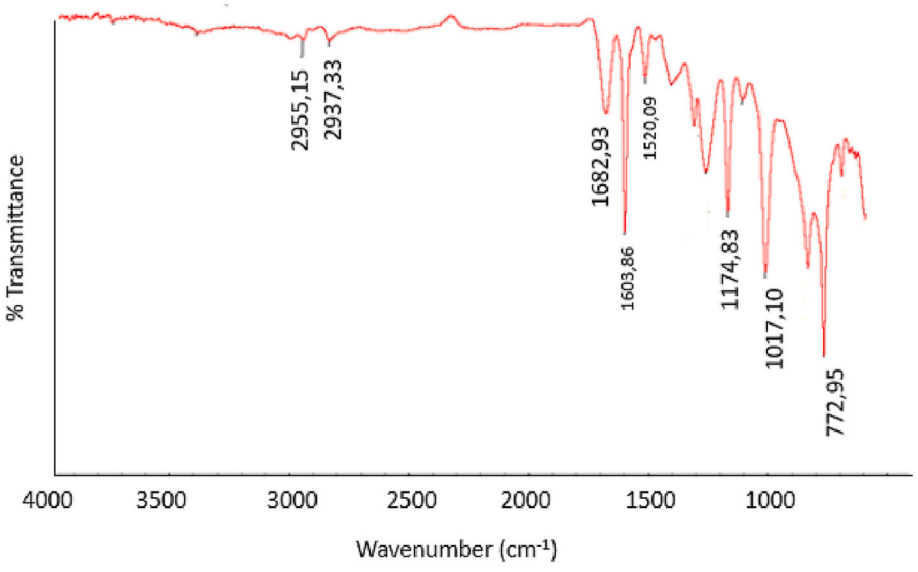

Fig. 4. FT-IR spectrum for Cell-ABA.

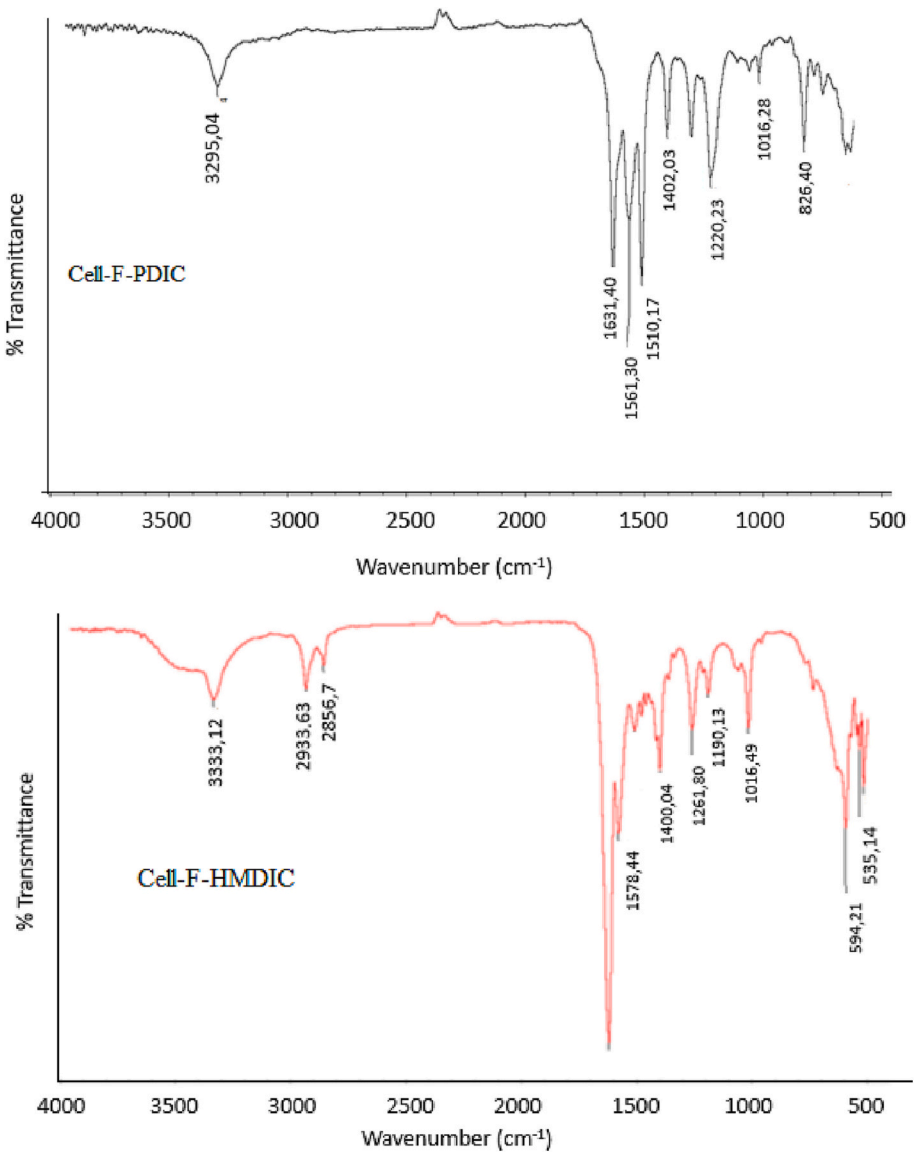

Fig. 6. IR spectra of Cell-F-PDIC and Cell-F-HMDIC.

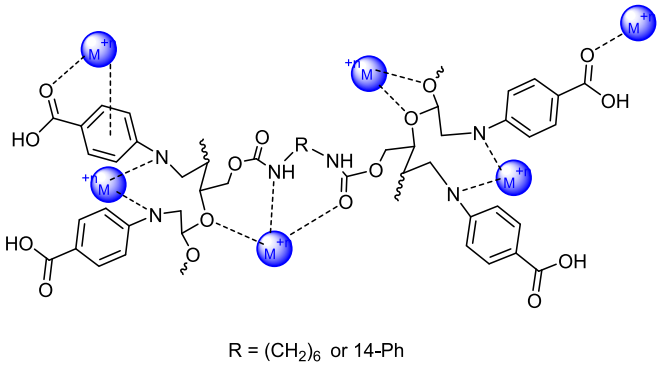

Fig. 7. A schematic diagram showing the binding sites in cellulose-based foam.

MX5 microbalance (thermostatic at 22 °C) heated to a temperature ranged from 25 to 1100 °C at a heating rate of 5 °C/min. The STARE software v.10.0 (Mettler Toledo) was used for controlled data analysis.

Initial and final concentrations of metal ion solutions were determined using Flame Atomic Absorption Spectrometer FAAS, ICE3500 AA System (Thermo Scientific, UK). Inductively coupled plasma mass spectrometry (CAP™ RQ ICP-MS) used in this work was purchased form Thermo Fisher Scientific (Waltham, MA, USA) was used in quantitative and qualitative analysis of wastewater. All performed analysis were done in triplicate. The *t*-test method was used in data analysis. All determined variations were statistically considered significant when the value of p term is lower than 0.05.

2.3. Preparation of Cellulose aminobenzoic acid (Cell-ABA)

Cellulose powder (10.0 g, 0.016 mol) was in a flask (1.0 L) with a half-liter of distilled water. The mixture was stirred for 2 h, then dosed with a 20 g (0.093 mol, 5.8 mol/AGU) sample of sodium periodate. The reaction container was covered completely with aluminum sheet to prevent photo-induced reduction of periodate. The reaction mixture was placed in a water bath at 40 °C and mechanically mixed for 24 h. The resulting dialdehyde cellulose was collected by suction filtration, washed (3 × 150 mL) with water and dried in the hood at room temperature [20].

A portion of CDA (1.00 g, 0.0117 mol)) was suspended in 50 mL of methyl alcohol, acetic acid (1 mL) was added to the mixture as catalyst

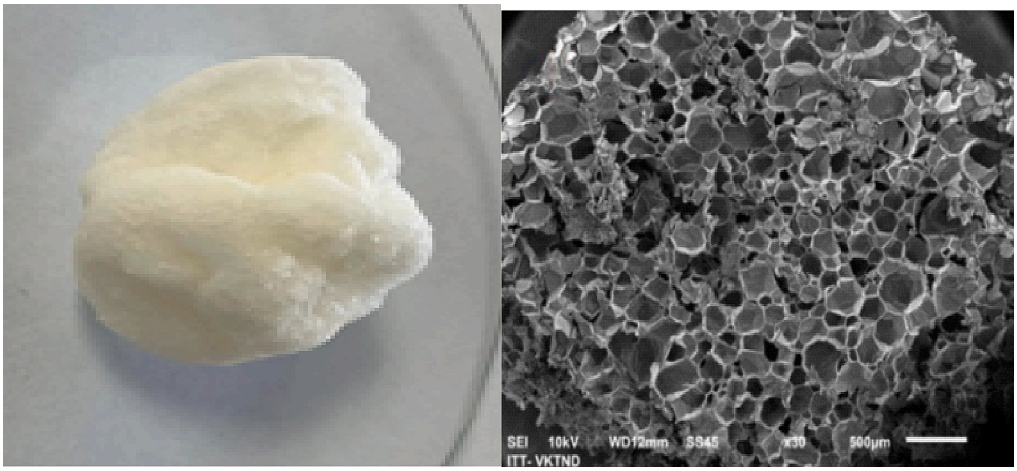

Fig. 8. Digital and SEM photographs of Cell-F-HMDIC.

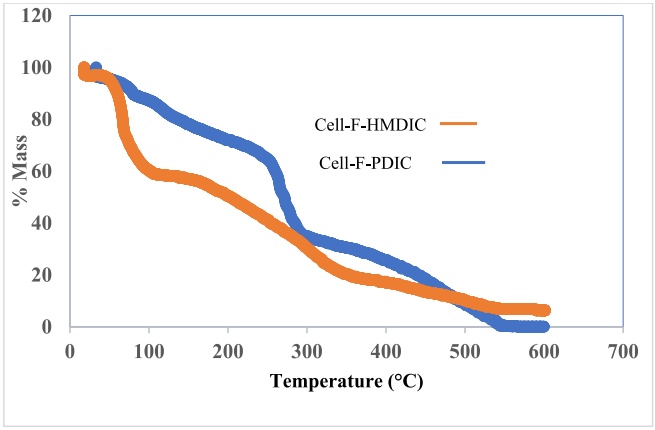

Fig. 9. TGA analysis results of Cell-F-HMDIC and Cell-F-PDIC.

followed with the addition of 4-aminobenzoic acid (1.2 g, 0.02 mol). The reaction mixture was stirred at 60 °C for 24 h. The resultant Schiff base was collected by suction filtration, washed several times with methanol. It was then transferred to a round bottom flask containing a 20 mL of MeOH. The produced suspension was treated with sodium borohydride (0.25 g) at room temperature for 10 min, then the temperature was increased to 60 °C, and kept at this temperature for 3 h. Residual sodium borohydride was eliminated by the addition of ice-cold water (5.0 mL), and the reaction mixture was filtered, and the collected product was washed with water, methanol, and dried in the hood.

2.4. Preparation of the cellulose based foam Cell-F-HMDIC and Cell-F-PDIC

A solution of 1,6-hexamethylene diisocyanate (1.0 mL, 0.06 mol) or 1,4-phenylene diisocyanate (1.0 g, 0.0625 mol) in 10 mL DMF was prepared, 3 drops of trimethylamine was added as a base to the solution. Cell-ABA (1.0 g, 0.0625 mol of AGU) was added to the solution and heated to 60 °C to initiate the reaction. Once an exothermic reaction started, the heat was turned off. A mass of foam was formed in about 10 min. The reaction was mixed for 60 min. The produced foam was then collected, washed with distilled water, methanol and dried at room temperature.

2.5. Adsorption study

Adsorption process was performed in plastic tubes with screw cover (50 mL each) that were clamped in a water bath furnished with a shaker and a thermostat. The effect of the parameters adsorbent dose, initial concentration of metal ions (C_0, ppm), mixing time (t, min), pH value, and temperature (T, °C) on adsorption efficacy was evaluated. Lead (II) was selected as a model ion for the adsorption experiments. A 10 mL plastic syringe was used to withdraw a sample during the adsorption experiment then filtered through a 0.45 μm syringe filter for analysis of residua metal by FAAS at 217 nm.

2.6. Water purification

A sample of wastewater obtained from a plant located in Jericho (Palestine) was filtered by passing it through plastic filter (a 0.45 μm) fitted on a 10 mL plastic syringe. The filtered sample was subjected to qualitative and quantitative analysis using ICP-AES (Water Center operated by An-Najah University, Palestine), the samples was used as a control. A 20 mL sample of wastewater was passed through a sample of foam (1.0 g, of Cell-F-HMDIC or Cell-F-PDIC) packed in a 50.0 mL syringe and analyzed by ICP-AES for leftover metal ions.

2.7. DFT calculations

The adsorbate (polymeric foams) and Pb(II) ions interaction energies were calculated using the DMol3 module of the Materials Studio software. To comprehend electrical interaction factor and correlation (DNP), the M06-L was combined with polarization techniques and a double numerical basis set [28–30]. The self-consistent field required a change in energy of less than 10–7 Ha to be met. In this investigation, the conductor-like screening model (COSMO) was utilized to describe the effects of water as a solvent [31,32].

2.8. Monte Carlo (MC) and Molecular Dynamic (MD) simulations

MD and MC simulations were used in the simulated adsorption process to explore the interaction between lead ions and the modelled foam surface. The environment is modelled after an adsorption process. The dimensions of the slab model that was utilized in the computations are as follows: 20.52 on each side by 55.53 Å on the height. The MC and MD computations were carried out inside of a simulation box that included 700 water molecules and one Pb(II) ion. For both the MC and MD calculations of the simulations, the widely known COMPASSII forcefield was employed [33–38]. The following settings were used in the MD: NVT ensemble, $T = 298.00$ K utilizing Berendsen thermostat (1 fs time step with a total duration of the simulation 700 ps) [39–41].

A Periodic Boundary Condition (PBC) slab of the Cell-F-HMDIC or Cell-F-PDIC was generated in the initial stage prior to Molecular

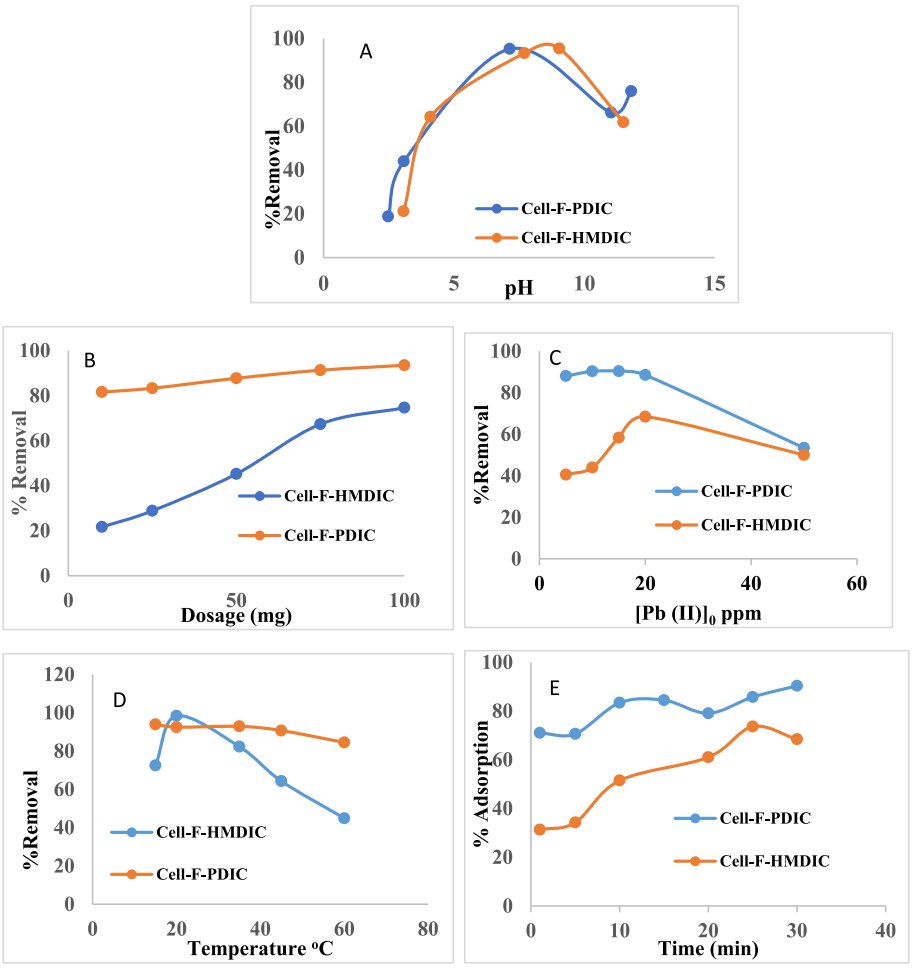

Fig. 10. The effect of various parameters on the removal (%) of Pb(II) by of the two foams (a) pH value (b) foam dose (c) initial [Pb(II)] (d) temperature (e) time.

Table 1
Foam adsorption efficiencies toward various metal ions present in sewage water.

Metal ions	Initial Concentration (ppm)	Foam adsorption Efficiency; % Removal	
		Cell-F-HMDIC	Cell-F-PDIC
Al	52.691	99.22	98.85
Ca	15.302	82.34	64.06
Co	0.029	99.79	95.017
Cr	0.372	56.79	75.69
Cu	1.564	97.05	97.7
Fe	69.821	98.07	90.71
Ga	0.031	80.64	71.612
Pb	0.159	95.43	90.49
Rb	0.284	71.77	47.59
Sr	5.401	81.73	56.86
Tl	0.003	92.8	96.8
U	0.025	90.08	85.16
V	1.211	54.72	27.40
Zn	8.819	98.07	98.24

Dynamic (MD) and Monte Carlo (MC) simulations. As shown in Fig. 1, the PCB has 8 chains of the matching adsorbate structures.

2.9. Adsorption

The lead (II) used in this study was chosen as a model metal ion. The adsorption process was carried out using the batch approach [42]. Adsorption was carried out at 25 °C using various amount of foam and solutions of metal ions with concentrations ranging from 40 to 50 mg/L.

Table 2
The isotherm parameters for the adsorption of Pb(II) ions by Cell-F-PDIC and Cell-F-HMDIC.

	Cell-F-PDIC	Cell-F-HMDIC
Langmuir isotherm		
Q^0 (mg/g)	2.1929	2.0345
K_L (L/mg)	0.1308	0.1162
R^2	0.8834	0.8372
Freundlich isotherm		
1/n	0.7149	0.8244
K_F (L/mg)	8.8795	8.6800
R^2	0.9867	0.9762

Adsorption time and pH effects were investigated, and the pH was altered by adding either HNO3 or NaOH. Thermodynamic parameters were used to assess the nature of the adsorption process.

The change in the metal ion content was monitored by AAS flame atomic absorption spectroscopy. Eqs. (1) and (2) were used to calculate the adsorption capacity of foam [14].

$$\%\text{removal} = \frac{C_0 - C_e}{C_0} \bullet 100 \quad (1)$$

$$Q_e = \frac{C_0 - C_e}{W} V \quad (2)$$

where C0 and Ce are the starting metal ion and the equilibrium metal ion concentration in ppm, respectively. The Qe is the equilibrium adsorption

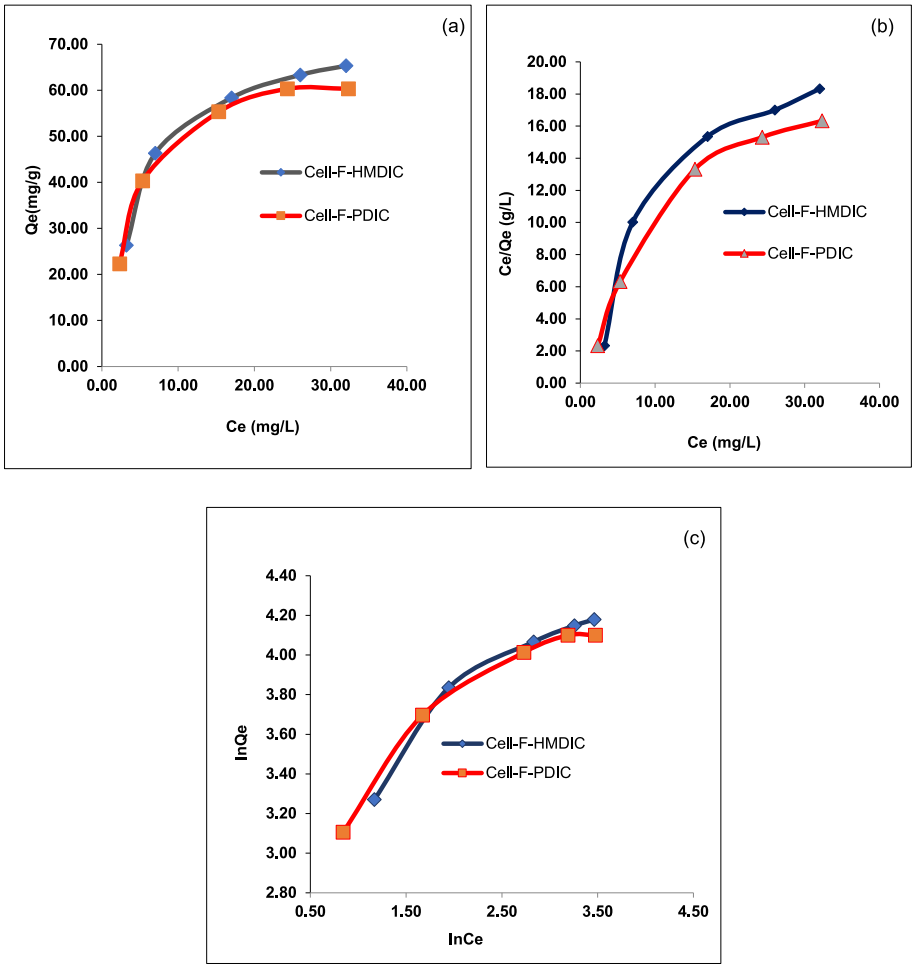

Fig. 11. Langmuir and Freundlich adsorption plots of Pb(II) ions on Cell-F-PDIC and Cell-F-HMDIC at different temperatures.

capacity in ppm, W is the weight in mg of the absorbent foam, and V is the volume in L of the solution.

where Co is the initial of metal ion, Ce is the and equilibrium concentration of metal ion in ppm, Qe is the adsorption capacity at equilibrium (ppm), W is the adsorbent foam weight (mg) of absorbent foam, and V is volume (L) of the analyzed solution.

2.10. Isotherm of the adsorption process

The Langmuir and Freundlich isotherm models were followed in this study to conclude the adsorption behavior of Pb(II) ions on Cell-F-HMDIC or Cell-F-PDIC surface [14]. The Langmuir isotherm model is presented in Eqs. (3) and (4):

$$\frac{C_e}{Q_e} = \frac{1}{q_{max}} C_e + \frac{1}{q_{max} K_L} \tag{3}$$

where Ce is the concentration of Pb(II) in ppm and Qe is the amount of metal ion extracted per unit mass of Cell-F-HMDIC or Cell-F-PDIC at equilibrium (mg/g), qax is the highest single layer adsorption capacity of the foam (mg/g), and KL (L/mg) represent Langmuir constant.

The Langmuir isotherm model can be used to forecast whether adsorption will be favorable or unfavorable using the dimensionless constant separation factor provided in Eq. (4).

$$\mathrm{RL} = \frac{1}{1 + K_L C_e} \tag{4}$$

where C0 stands for the initial [Pb(II)] and KL stands for the Langmuir constants. If the RL value exceeds one, the adsorption is deemed to be unfavorable, favorable, or linear if it is between one and one.

The Freundlich isotherm model shown in Eqs. (5) and (6) symbolizes the heterogeneous surface energy non-ideal adsorption process.

$$ln(q_e) = lnk_f + \frac{1}{n} lnC_e \tag{5}$$

$$\mathrm{Qe} = \mathrm{K_F\ C_e 1/n} \tag{6}$$

where 1/n is the adsorption intensity and KF stands for a constant that denotes the relative adsorption capacity [38,39]. Adsorption is advantageous if 1/n is between 0.1 and 0.5; it is unfavorable if 1/n is more than.

2.11. Kinetics of the adsorption process

The rates of Pb(II) adsorption on the Cell-F-HMDIC and Cell-F-PDIC surfaces were examined using the pseudo first-order and second order kinetic models shown below. The linearized versions of the rate equations were calculated using Eqs. (7) through (10) [38,39].

$$ln(q_e - q_t) = lnq_e - \mathrm{K1\ t} \tag{7}$$

$$\frac{\mathrm{t}}{\mathrm{q_t}} = \frac{1}{\mathrm{K_2} q_e^2} + \frac{\mathrm{t}}{\mathrm{q_e}} \tag{8}$$

$$\mathrm{Q_t} = \mathrm{K_{id}} \mathrm{t}^{1/2} + \mathrm{Z} \tag{9}$$

Table 3
Parameters obtained by the kinetic models for the foams Cell-F-PDIC and Cell-F-HMDIC.

		Cell-F-PDIC	Cell-F-HMDIC
Pseudo-first-order kinetic model			
$\mathbf{K_1}$ (g/mg·min)		0.087	0.056
$\mathbf{Q_{cal}}$ (mg/g)		10.878	10.990
R^2		0.988	0.853
The pseudo-second-order parameters			
$\mathbf{K_2}$ (g/mg.min)		0.142	0.268
$\mathbf{Q_{cal}}$ (mg/g)		4.541	3.977
R^2		0.966	0.981
Intra-particle diffusion parameter			
$\mathbf{K_{id}}$		27.288	27.678
Z		0.814	1.8557
$\mathbf{R^2}$		0.847	0.8512
Liquid film diffusion model			
K_{df}		2.1423	2.0931
R^2		0.9459	0.9184
Parameters values for the adsorption			
	T(K)		
	298	−21.517	−20.224
ΔG° (KJ/mol)	**313**	−22.602	−21.247
	323	−23.326	−21.927
ΔH° (KJ/mol)		39.8195	39.3952
ΔS° (J/K·mol)		72.3405	68.009

$$ln\frac{K(T_2)}{K(T_1)} = \frac{Ea}{R} \bullet \left(\frac{1}{T_1} - \frac{1}{T_2}\right) \quad (10)$$

$$\mathrm{Ln}(1 - \mathrm{F}) = -\mathrm{K_{fd}}^{*}\mathrm{t} \quad (11)$$

where Qt is the temperature-dependent adsorption capacity and qe is the equilibrium adsorption capacity (mg/g). K1 stands for the pseudo-first-order rate constant (min), and K2 for the pseudo-second-order rate constant (g/ mg.min). Z (mg/g) can be used to determine the boundary layer thickness, where Kid is the diffusion rate constant measured in mg/g.min1/2. In Eq. (11), kfd (min1) stands for the rate of film diffusion, and F represents the fractional accomplishment of equilibrium (F = qt/qe).

Eqs. (12) through (14) were used to compute the enthalpy (ΔH°), Gibbs energy (ΔG°), and entropy (ΔS°).

$$\mathrm{K_c} = \mathrm{C_{ads}}/\mathrm{C_e} \quad (12)$$

$$\Delta \mathrm{G}^0 = -\mathrm{RTlnK_c} \quad (13)$$

$$lnK_s = \frac{\Delta S}{R} - \frac{\Delta H}{RT} \quad (14)$$

where T is the solution temperature (K), R is the ideal gas constant (J/mol K), Cads is the equilibrium Pb(II) adsorbed quantity (mg/L), Ce is the equilibrium concentration (mg/L), and T is the thermodynamic constant (Kc) [38,39].

3. Results and discussion

3.1. Cellulose dialdehyde (Cell-DA)

Cellulose powder used in this study was extracted from the waste material of the olive oil industry. And purified according to a published process [20]. It was purified using the Kraft pulping process with some modifications regarding the concentration of NaOH and Na2S used in the process [20]. The extracted cellulose was subjected to a whitening process using various bleaching chemicals such as hydrogen peroxide and sodium hypochlorite. Obtained cellulose was converted to cellulose dialdehyde (Cell-DA) by oxidizing it with sodium periodate as shown in Fig. 2 [42]. The reaction was performed at 45 °C for 12 h, no adjustment on the pH value was made to the reaction mixture (pH = 3.7). Analysis of the produced Cell-DA by FT-IR showed the presence of the expected peaks (Fig. 2) 1728 cm^{-1}, 1424 cm^{-1}, 1373 cm^{-1}, and 1142 cm^{-1} corresponding to C═O of aldehyde group, asymmetric bending of CH2, stretching of ether of glycosidic linkage (C-O-C) and C—O of alcohol, respectively. The band at 1732 cm^{-1} corresponding to C═O was not intense, which could be related to the formation of acetal by hydration [43].

3.2. Amination reaction of 2,3-dialdehyde cellulose through Schiff's base formation

The tendency of cellulose to undergo modification reaction increases as the hydroxyl groups are converted to aldehydes. The generated Cell-DA was derivatized with the aromatic amine p-aminobenzoic acid to produce the cellulose Schiff base Cell-ABA, as shown in Fig. 3 below. The reaction was performed in methanol at 60 °C for 24 h. The reaction represents a condensation reaction that starts with nucleophilic attack of an amine at the carbonyl carbon, followed with a water elimination and formation of Schiff base. Reductive amination of the produced imine was performed using sodium borohydride.

The change in the functional group was detected by FT-IR (Fig. 4), which represents the IR spectrum of the Cell-ABA. The IR spectrum shows the disappearance of the peak corresponding to the C═O (1732 cm^{-1}), and the existence of the C═O of carboxyl group. The C═C of benzene ring appear at 1682 and 1602 cm^{-1}, respectively. The O—H stretching peak of the carboxylic acid group appear as a broad peak extends from 3366 cm^{-1} to 2600 cm^{-1} [44,45].

3.3. Cellulose-based polyurethane foam with ionic group

One of the most common PUF preparation techniques involves using diisocyanate for the formation of a polycondensation reaction between diol and diisocyanate [42]. Diisocyanates suitable for use could be aliphatic or aromatic. For comparison purposes, in this study, two different polymers were prepared via reacting the final product with aliphatic and aromatic diisocyanate compounds. The foam preparation was performed in dimethyl formamide by reacting cellulose amine derivatives with the hexamethylene diisocyanate in presence of triethyl amine base to form the aliphatic foam Cell-F-HMDIC, and with 1,4-phenylene diisocyanate to form the aromatic foam Cell-F-PDIC. A representative diagram summarizing the reaction is shown in Fig. 5.

The IR spectra of both foams Cell-F-HMDIC and Cell-F-PDIC are shown in Fig. 6. Both spectra show the N—H stretching band at about 3300 cm^{-1}. The peaks at 1630 cm^{-1} could be related to the C═O of the urethane. C═C stretching band of aromatic group of Cell-F-PDIC appears at 1561 cm^{-1}. C—H stretching band was also observed at 2933.63 cm^{-1} corresponding to the methylene of Cell-F-HMDIC. The vibration band of C—O alkoxy was observed at 1261.8 cm^{-1}.

The cellulose-based foams were designed to contain many sites with high affinity for metal ions (Fig. 7). The metal binding sites include carbonyl, carboxyl, amine, aromatic and hydroxyl groups.

A photo and a SEM image of the Cell-F-HMDIC foam are shown in Fig. 8. Both images show highly porous and spongy structure. This could be related to the presence of the polyurethane functionality. This spongy morphology makes the polymer accessible and adds a filtering capability to the foam.

3.4. Thermal analysis

The prepared two foams were subjected to thermal analysis the obtained results are summarized in Fig. 9. Both foams show almost similar

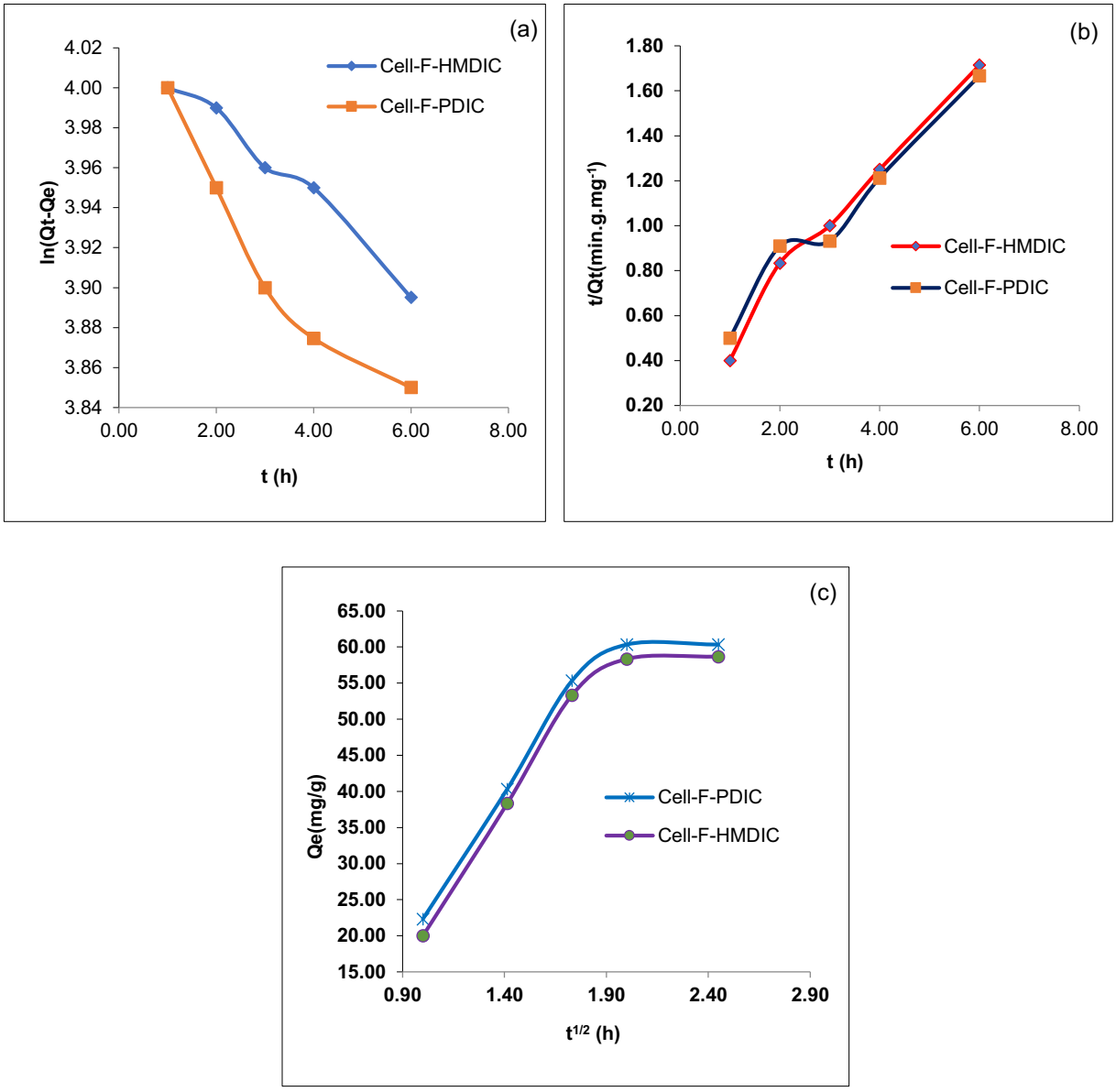

Fig. 12. Kinetic plots of lead(II) adsorption by foams a) Pseudo first-order, b) Pseudo-second order, and c) Intraparticle diffusion model.

trend regarding thermal decomposition. A high mass loss started at 200 °C, which could be attributed to the loss of the side groups. A major degradation started at 400 °C which could be related to the degradation of the cellulose chain. The foams is considered a stable for performing water purification form metal and organic matter.

3.5. Adsorption of Pb(II)

A batch adsorption method was conducted to test the efficacies of the synthesized foams for heavy metal removal, and to determine the optimum conditions for heavy metal adsorption. Pb(II) was selected as a model ion for the adsorption experiments.

3.5.1. Effects of various parameters

3.5.1.1. Effect of pH. Solution pH is a main factor since the during the variation in this factor the receptor sites could be activated for binding or blocked. The study was carried out on a 10 mL solution of adsorbate at room temperature using a 25 mg foam for 30 min. The results are shown in Fig. 10a. At low pH (at about 2.5) both the carboxyl and the amine groups are present in their protonated forms, this could reduce their affinity for heavy metal. As a result, the adsorption efficiency drops significantly at low pH. As the pH increases, however, the amine and carboxyl groups start to shift from their Lewis acid forms to their Lewis base forms, which convert them from weak chelating agents to strong chelating agents. This could be related to the lone pairs of electrons present on N and O. The highest adsorption efficacy occurred at a pH of 7.5. At pH values greater than 8.0, the adsorption efficacy started to decline. The decline could be related to the generation of metal oxide that is soluble in aqueous solutions.

3.5.1.2. Effect of adsorbent dose. The scheme depicted in Fig. 10b displays the impact of adsorbent foam dosage on removal percentage. Foam adsorbents were utilized in various concentrations of Pb(II) ranging from 5.0 mg to 50.0 mg, while the other variables remained constant at 10.0 mL of solution volume, 15.0 ppm of initial Pb(II) concentration, and a pH valued of 4.3. The mixtures were mixed for 30 min at room temperature. The findings demonstrate that raising the foam dosage increases the amount of metal removed. It was found that at a dosages of 25 mg the maximum Pb(II) reductions were about 95.0 % and 75 % for

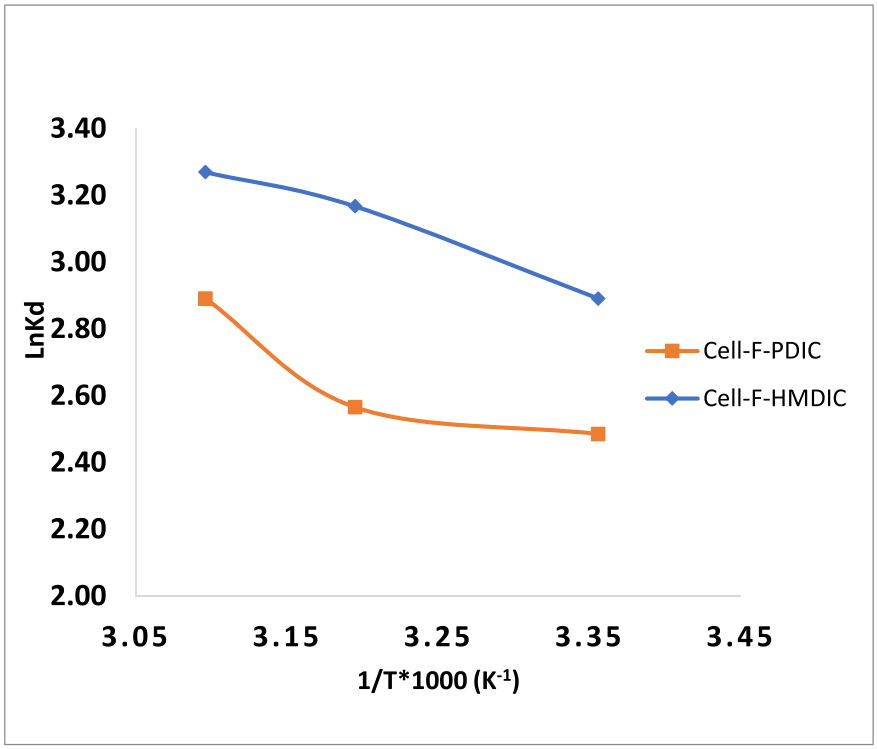

Fig. 13. Adsorption thermodynamics of Pb(II) ions onto Cell-F-PDIC and Cell-F-HMDIC.

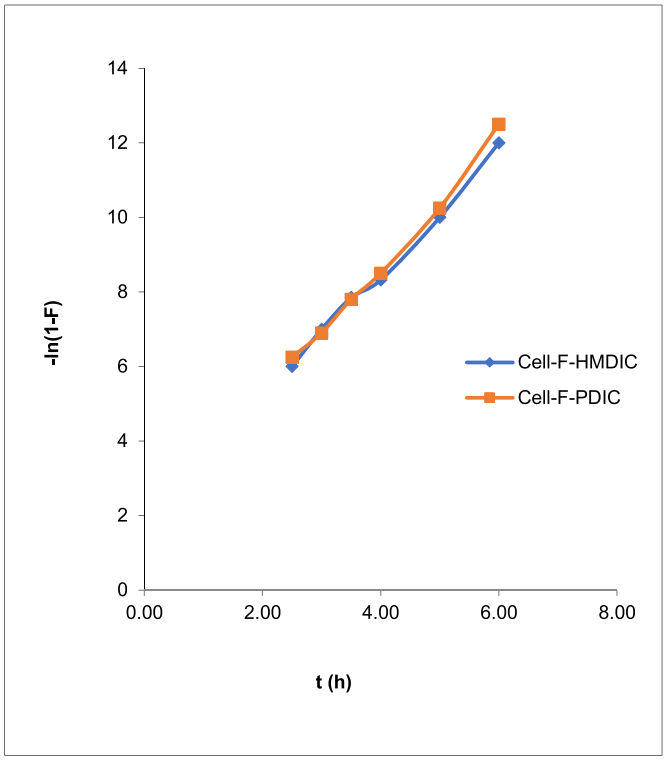

Fig. 14. Plot of Liquid film diffusion model for the adsorption of Pb(II) by Cell-F-PDIC and Cell-F-HMDIC

Cell-F-PDIC and Cell-F-HMDIC, respectively,.

3.5.1.3. Effect of metal ion concentration. The effect of the lead ions concentration on rate of removal was investigated while the other parameters were kept constant: solution volume, pH, time, temperature, and foam dose were kept constant at 10 mL, 4.3, 30 min, 25 °C and 15 mg, respectively. The maximum removal was 70 % and 90 % for the foams Cell-F-HMDIC and Cell-F-PDIC, respectively (Fig. 10c). At an initial concentration higher than 20 ppm both foams showed a drop in the adsorption efficacy. The results depicted in Fig. 10c show that at a concentration of 20.0 ppm or lower, there are Meta receptors, and the adsorption process is regulated by ion diffusion mechanism [46]. At a concentration higher than 20 ppm, the availability of the metal receptors starts to decline as a result of saturation, which also causes the adsorption efficacy to drop.

3.5.1.4. Temperature effect on adsorption. The percent removal of Pb(II) as a function of temperature was studied in the range of 15 to 45 °C. The highest removal was obtained at room temperature as shown in Fig. 10d. However, the efficiency for Cell-F-HMDIC dropped as the temperature increased to 45 °C, which indicates that the adsorption is exothermic and requires no heat. The other foam (Cell-F-PDIC) showed a little drop in the efficiency as the temperature raised from room to 45 °C. This could be attributed to the presence of the aromatic rings since aromatic complexation might require some heat, as reported in the literature. The metal ions tend to form sandwich type of complexes with aryl groups.

3.5.1.5. Effect of contact time. The effect of the contact time on rate of removal of Pb(II) was determined while the other parameters such solution volume, pH, initial concentration of Pb(II), temperature, and foam dose were kept constant at 10 mL, 7.5, 20 ppm, 25 °C and 15 mg, respectively. Fig. 10e shows that the % removal of Pb(II) increased with time, then at 30 min period it tends to become constant. The results could be explained based on the availability of the metal receptors, which decreases with time due to adsorption, at about 30 min almost all metal receptors are engaged [47].

All results indicate that Cell-F-PDIC has a higher metal adsorption capacity than Cell-F-HMDIC. The polymer rigidity due to the presence of more aromatic pendant groups could be the reason for this finding. In addition, aromatic rings considered binding sites for metal ion, thy tend

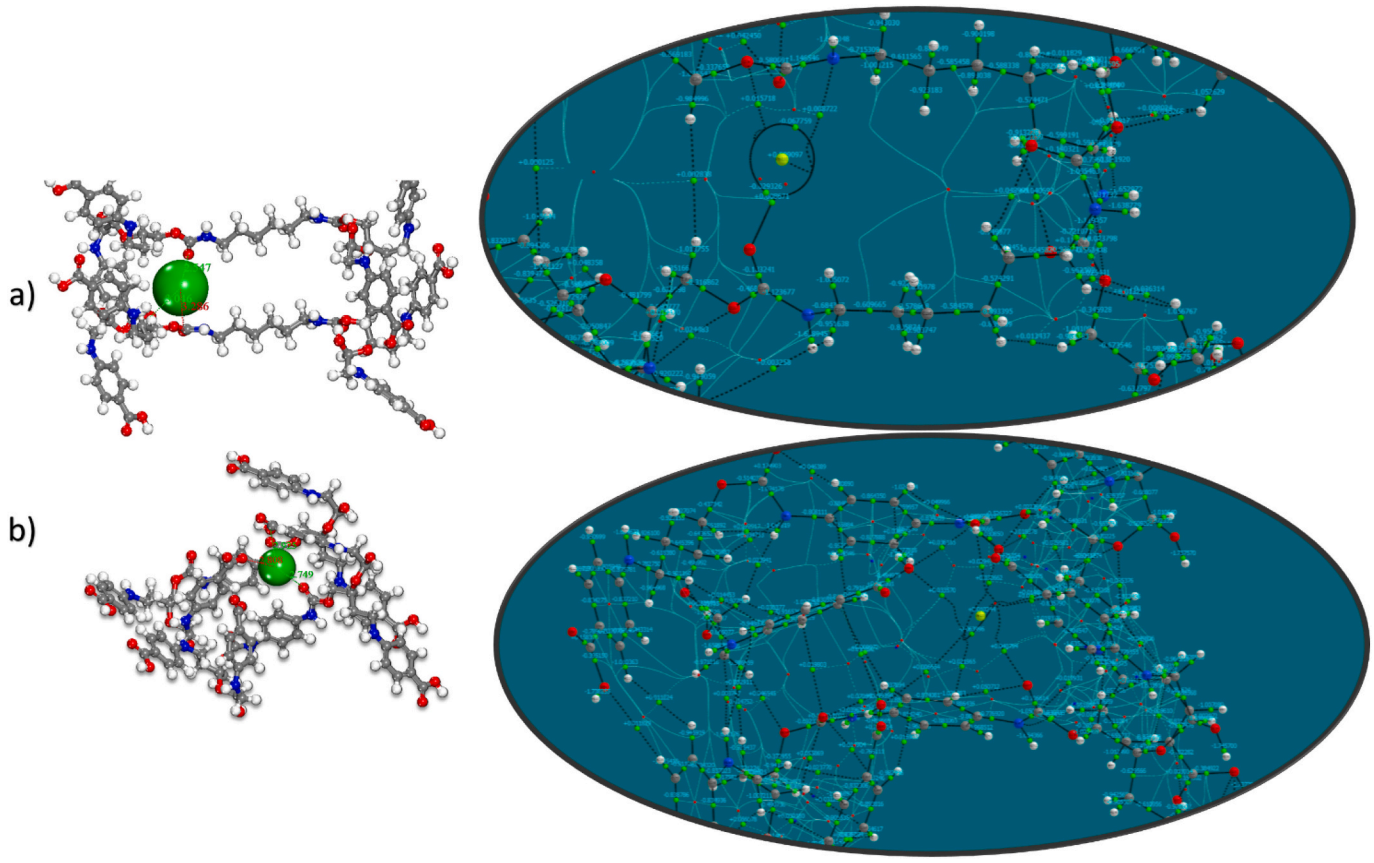

Fig. 15. DFT final geometries and corresponding molecular graphs derived from Quantum Theory of Atoms in Molecules (QTAIM) study.

to form with metals sandwich type of complexes. The presence of the long aliphatic group (hexyl) causes the polymer to fold. Polymer folding reduces the number of exposed metal biding sites thus reduces the efficiency.

3.6. Wastewater purification from metals

Contaminated water samples were taken at the Jericho wastewater treatment facility in Palestine. The produced foams were applied to two samples of the collected water in accordance with the established ideal adsorption conditions. ICP-MS was used to calculate the metal ion concentrations in ppm before and after treatment with the foams. Table 1 displays the results in summary. The obtained results showed that, with regard to practically all metal ions included in the sewage samples, both foams demonstrated outstanding adsorption efficiencies.

3.7. Adsorption analysis

3.7.1. Isotherm

The Langmuir (Eq. (3)) and Freundlich isotherm (Eq. (5)) models were followed to determine the adsorption equilibrium between the Pb (II) ion and the two foams Cell-F-PDIC and Cell-F-HMDIC in water [15]. They were also utilized to assess the metal ion dispersion on the Cell-F-PDIC and Cell-F-HMDIC surfaces at equilibrium. One of the factors that may affect the type of isotherm followed in the adsorption is the correlation coefficient (R^2) [15].

Data listed in Table 2 represents the values of all adjustable parameters obtained from Fig. 11. As shown in Table 2, the obtained data showed that the correlation coefficients obtained using Freundlich isothermal model are lower, demonstrating that lead cations adsorption adheres to the Freundlich equation, in which Pb(II) cations are dispersed uniformly and evenly over the foam porous surfaces. For various dosages of foam adsorbent, the separation factor RL ranges from 0 to less than1 (Table 2). This demonstrates the great affinity of Cell-F-PDIC and Cell-F-HMDIC for the relevant metal ions.

3.7.2. Adsorption kinetics of Pb(II) ions on Cell-F-PDIC and Cell-F-HMDIC

The Pb(II) ion adsorption by the Cell-F-PDIC and Cell-F-HMDIC foams was analyzed using various kinetic models to understand the nature of the adsorption mechanism. Pseudo-first and pseudo-second order models, two of the most popular kinetic models, were followed to simulate the metal adsorption by the foam adsorbents. The used kinetic models are depicted in Eqs. (7) and (8) [15].

The equations parameters values are shown in Table 3 and Fig. 12. The value of K1 is provided by the plots of Ln (qe-qt) versus t (Fig. 12a), while the values of K2 and the adsorption capacity qe are provided by the slope and intercept of the plot of t/Qt versus t (Fig. 12b), and Kid and Z were calculated by plotting Qt versus t1/2 (Fig. 12c).

The results obtained from the experimental part reveals that the value of R^2 for the pseudo-second order (0.9663 to 0.9815) is higher than that obtained by the pseudo-first order (0.9881to 0.8532) on the Cell-F-PDIC and Cell-F-HMDIC, respectively. The computed qe values (4.5414 mg/g) are close to the observed qe values (3.977 mg/g) the Cell-F-HMDIC, for the pseudo-second order model. The values indicate that the Pb2+ adsorption on the foam surfaces conforms the pseudo-second order model (Table 3 and Fig. 12b).

Kid and Z were calculated from Fig. 12c (Qt vs. t1/2), there values are shown in Table 3. Several rate-limiting processes present could be available for the adsorption process, since all the graphs shown in Fig. 9 are straight lines and that do not cross their respective origins.

We may infer from the initial graphs linearity in Fig. 12b that Pb(II) adsorption on Cell-F-PDIC and Cell-F-HMDIC foams starts with an instantaneous adsorption on the external surface, which results in a chemical complexation between Pb(II) and surface functional groups

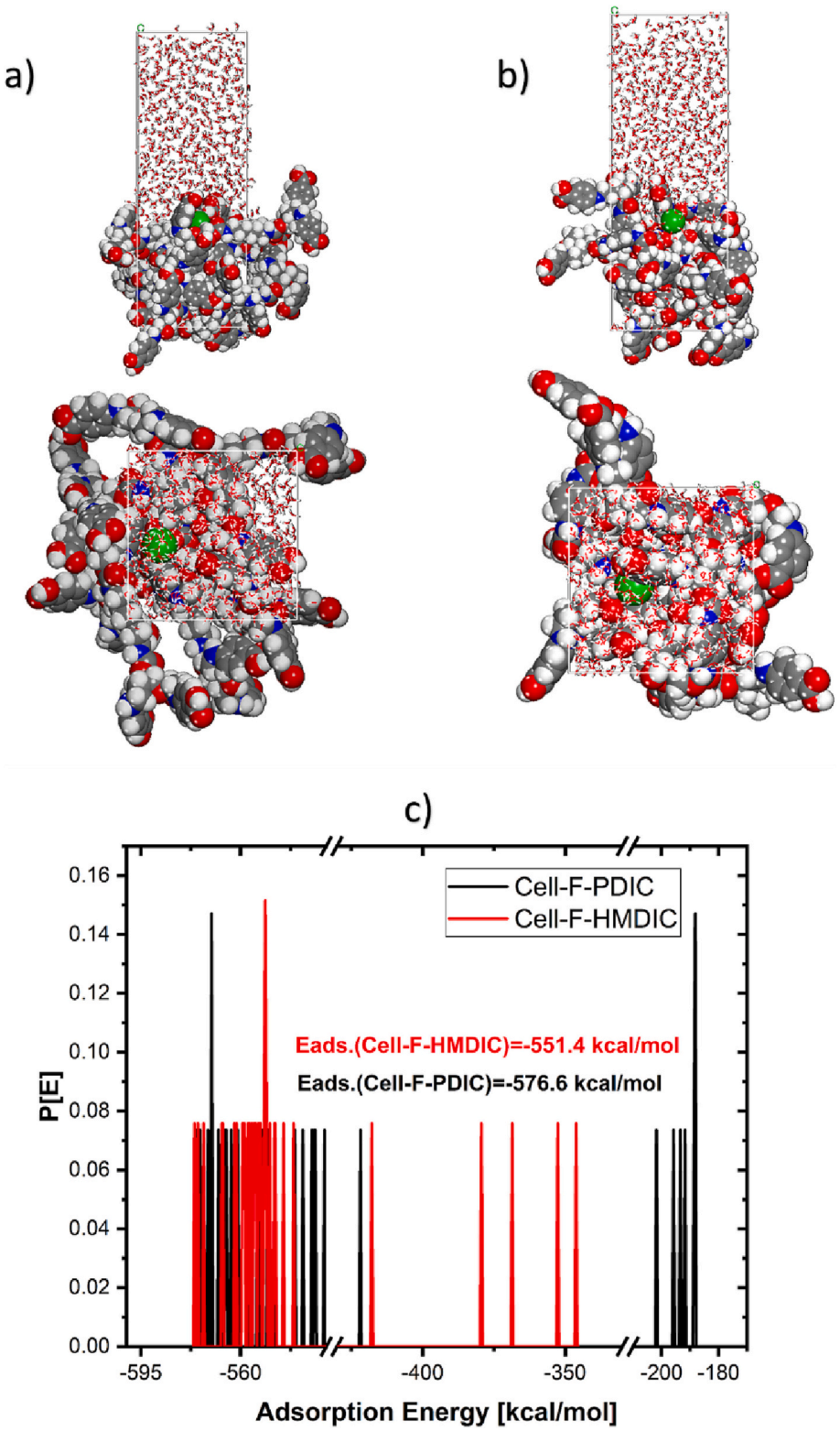

Fig. 16. a, b) the lowest energy geometry of the simulation box as obtained from MC and c) the adsorption energy distributions probability during MC for the Pb(II) ions onto Cell-F surfaces.

[38,39]. The other steps were also linear, showing that Pb(II) ions were gradually adsorbing and that the rate of intraparticle diffusion was being constrained.

Table 3 demonstrates that while the outside mass transfer potential decreased and the top layer expanded, the inner mass transfer potential increased. Eq. (9) was used to determine the energy of activation of the adsorption at 298 and 323 K.

These results help explain how temperature impacts the Pb(II) ion's ability to adsorb on Cell-F-PDIC and Cell-F-HMDIC. The nearly nonexistent activation energy calculated suggested a spontaneous adsorption mechanism.

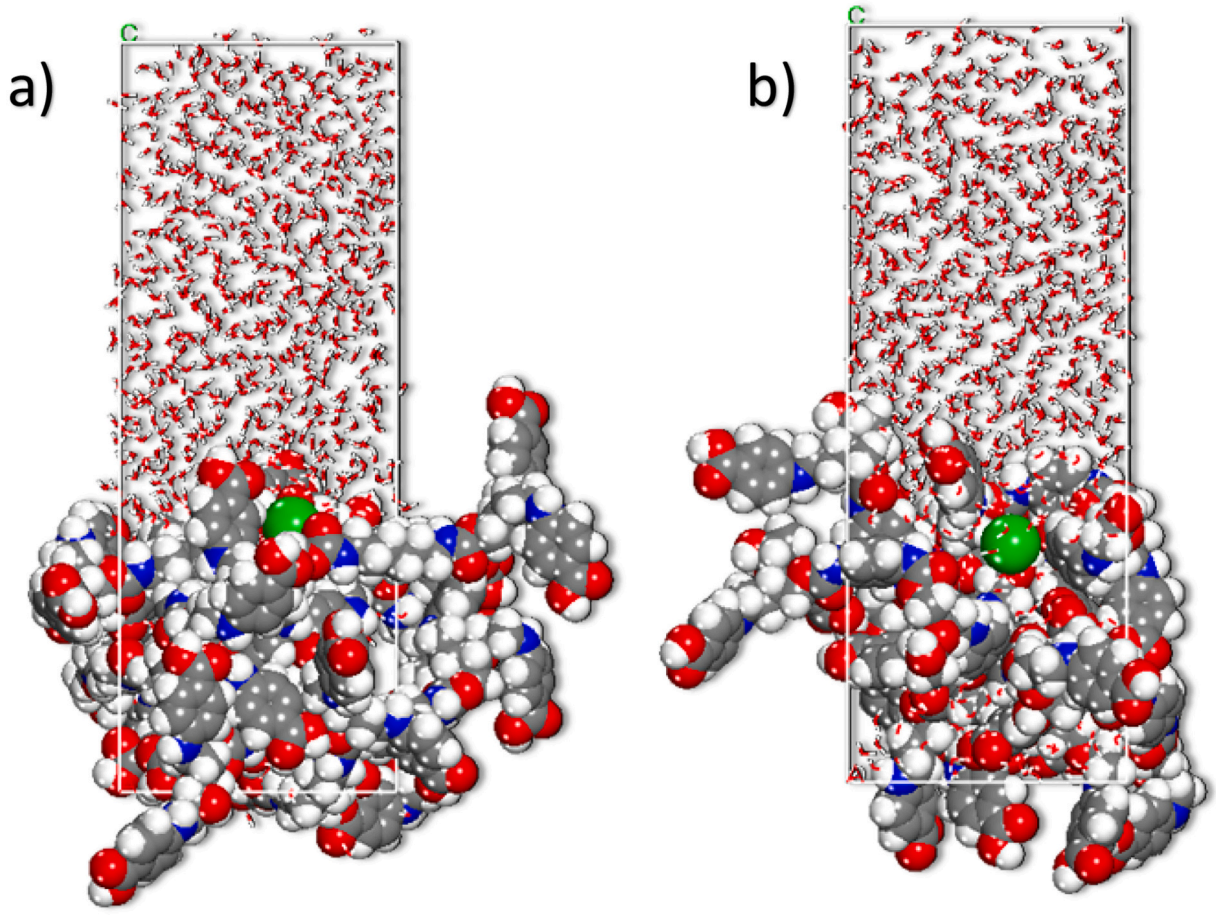

Fig. 17. The geometry of the lowest bonding energy poses obtained from MD for the adsorbate molecules onto the Cell-F (a. Cell-F-HMDIC and b. Cell-F-PDIC) surfaces.

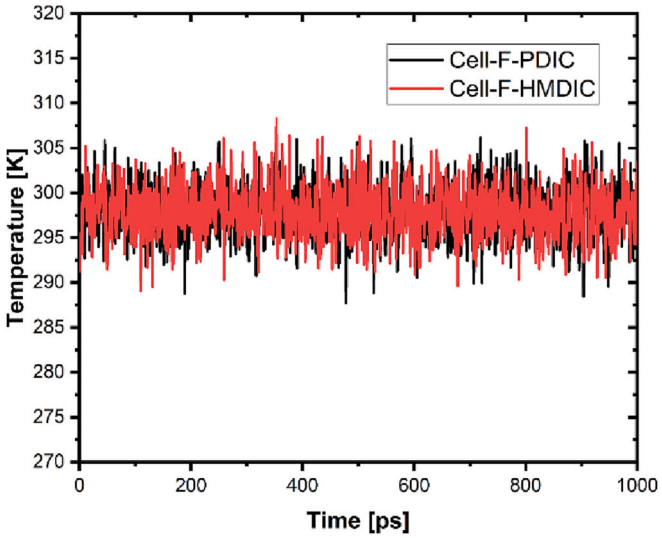

Fig. 18. Temperature change during the course of the MD simulation.

3.8. Thermodynamics study

To comprehend spontaneity and the sort of adsorption, the values of the parameters: standard free energy, standard enthalpy, and standard entropy were estimated.

The value of ΔG0 (J/ mol) was obtained using Eq. (12). Fig. 13 shows the mapping of the ln Ks vs. 1/T. Table 3 lists the different thermodynamic parameters that were calculated using the slopes and crossings.

The results for ΔS0 and ΔH0 are positive, and the adsorption process is what raises the entropy at the solid/solution contact. Additionally, the Cell-F-PDIC and Cell-F-HMDIC both had negative free energies, which pointed to a spontaneous uptaking process at wide range of temperatures.

Adsorption is typically used to remove metal in phases. Metal ions move from most of the solution to the outer surfaces of the Cell-F-PDIC and Cell-F-HMDIC in the first step, then diffuse across the boundary layer to those surfaces, that initiate the metal ion adsorption at the coordination sites located at the surface of the foams Cell-F-PDIC and Cell-F-HMDIC, at the end intraparticle diffusion across the Cell-F-PDIC and Cell-F-HMDIC particles occurs flowed by more adsorption. Further investigation was done using the liquid film model and the intraparticle diffusion model to get a detailed picture about the adsorption mechanism.

The movement of metal ions through a liquid film enclosing the foam adsorbent is the longest phase of the adsorption process, according to the liquid film diffusion model. Described in Eq. (15).

$$ln(1 - F) = k_{fd}\, t \quad (15)$$

where F is the fractional equilibrium achieved. The film-diffusion coefficient is kfd (min-1), and its formula is (F = qt/qe).

If equation shows that the plot of ln(1 - F) versus t produced a straight line that if possess through the origin, then adsorption process includes diffusion through a liquid film around the Cell-F-PDIC and Cell-F-HMDIC. Qe is the equilibrium (mg/g) adsorption capacity (Fig. 14).

The graph shown in Fig. 14 didn't exhibit linear lines crossing the origin, and had extremely low R2 values of 0.9459 and 0.9184 for Pb(II), respectively. This suggests that the step determining velocity was not diffusion of ions via the liquid film surrounding the Cell-F-PDIC and Cell-F-HMDIC. These results suggest that, although not the slowest stage in determining the rate, the liquid film's diffusion pattern may have an impact on the adsorption of lead(II) by foam, especially at the beginning of adsorption, as presented in Table 3.

3.9. Theoretical results

3.9.1. DFT results

The final geometries of the matching pairs of Pb(II) adsorbate structures are depicted in Fig. 15. The interaction energy of the Pb(II) ions is comparable for both of the adsorbate structures as estimated from DFT. The value for Cell-F-HMDIC/Pb(II) is −141.38 kcal/mol, while the value for Cell-F-HMDIC/Pb(II) is −143.50 kcal/mol.

The integration of electron density over Bader atoms was the focus of an AIM investigation that was carried out. On the bond critical points (BCPs) binding the Pb(II) cation and oxygen atoms, critical points were identified, and local or integrated characteristics were calculated. The findings point to a significant amount of ionic character within the metal–ligand Pb—O binding leading to the adsorption of these ions onto Cell-F adsorbent [48,49]. First, the presence of closed-shell interactions may be deduced from the low electron density (ρBCP ≈ 0.03 a.u.) and positive values of the laplacian (∇2ρBCP 0.06–0.16 a.u.) [50].

3.9.2. Monte Carlo (MC) and Molecular Dynamic (MD) simulations

Monte Carlo simulations involve randomly sampling the potential energy surface of a system to simulate the behavior of molecules. In this method, the system is treated as a collection of interacting particles, and the positions and velocities of these particles are randomly changed in order to calculate the potential energy of the system. The simulation proceeds by sampling many possible configurations of the Pb(II) adsorption configuration on the Cell-F surface that is the most efficient. and calculating the probability of each configuration occurring (Fig. 16).

In this method, the computation of the adsorption energetics is made possible because to the interaction of the molecules of the adsorbate with the surface of the lead(II). Quantitatively speaking, this is accomplished by using the following equation to get the adsorption energy (Eads) [50–53]:

$$E_{ads} = E_{Cell/Pb(II)} - \left(E_{Cell-F} + E_{Pb(II)}\right) \quad (16)$$

The experiment's results are supported by the fact that the adsorbate ions introduced on both Cell-F surfaces possessed a much greater negative value of Eads [54–56]. In MD simulations, the method for calculating and documenting the dynamics of adsorbate on the modelled material's surface is employed [37–39,57]. During the course of MD, the ultimate structure of the adsorbate ions as they reside on the Cell-F surfaces is seen in Fig. 17.

Checking for and accounting for any changes in temperature that take place while the MD simulation is being carried out is one way to ensure that the energy content of the molecules is as low as is feasibly conceivably able to be. This is one way to ensure that the energy content of the molecules is as low as is feasibly able to be [37,39,58]. The fact that there is no apparent change in temperature, as shown in Fig. 18, is evidence that the MD that we utilized in our system worked effectively [59,60].

Because of their relatively high adsorption negative energy value and their proximity to the Cell-F surfaces, Pb(II) ions perform to have vigorous interactions with the adsorbate surface [41,56] [47, 71]. This is demonstrated by the fact that the Pb(II) ions are positioned fairly adjacent to the Cell-F surfaces.

4. Conclusion

The current study represents a novel method for converting the agricultural solid waste material to a novel polymeric foam with commercial application. The solid waste of the olive industry (OISW) was used as a source of cellulose powder which was converted in a four-step method to foam with ionic receptor sites. The method involved introducing dialdehyde functionality on the repeat unit of cellulose by oxidation with periodate, reacting cellulose with dialdehyde functionality with the aromatic amino acid 4-aminobenzoic acids to form a Schiff base, reduction of the Schiff base with sodium borohydride, then converting it into foam by polymerizing it with hexamethylene diisocyanato and *p*-phenylene diisocyanate. The prepared polymers and foams were characterized by SEM, TGA, and FT-IR. The produced foams were used in wastewater purification form toxic metal ions. Optimum adsorption conditions were determined. Quantitative removal of several metal ions from sewage sample was achieved. Kinetic study revealed that the adsorption of the metal ion Pb(II), which was used a model ion, follows the pseudo second order kinetics. Thermodynamic study revealed negative Gibbs free energy values, indicating a spontaneous coordination of Pb(II) to foam surface. Theoretical computation using Monte Carlo (MC) and Molecular Dynamic (MD) simulation models showed excellent affinity of prepared foams for the model ion Pb (II) with highly negative adsorption energy values indicating vigorous interactions of Pb (II) with the adsorbate surfaces.

Declaration of competing interest

The authors declare that they have no known competing financial interests or personal relationships that could have appeared to influence the work reported in this paper.

Acknowledgments

This study was supported by The Scientific and Technological Research Council of Turkey (TUBITAK) and The Higher Council for Innovation and Excellence of Palestine (HCIE), 2521 International Bilateral Research Project (Grant Number: 120N633), and the authors gratefully acknowledge TUBITAK and HCIE. The authors are gratefully acknowledging the support from the Ministry of Education, Science and Technology of Kosovo (Nr.2-5069) for providing the computing resources.

References

[1] S.Abdurrahman Abubakar Shawai, A review on heavy metals contamination in water and soil: effects, sources and phytoremediation techniques, IJMPEM 2 (2017) 21, https://doi.org/10.11648/j.ijmpem.20170202.12.
[2] A.C.Gonçalves Junior, D. Schwantes, E.Conradi Junior, J. Zimmermann, G. F. Coelho, Adsorption of Cd (II), Pb (II) and Cr (III) on chemically modified Euterpe Oleracea biomass for the remediation of water pollution, Acta Sci Technol. 43 (2020), e50263, https://doi.org/10.4025/actascitechnol.v43i1.50263.
[3] A. da Paz Schiller, M.C. Ferronato, D. Schwantes, A.C. Gonçalves Jr., D.J. Barilli, J. Manfrin, Influence of hydrological flows from tropical watersheds on the dynamics of Cu and Zn in sediments, Environ. Monit. Assess. 191 (2019) 86, https://doi.org/10.1007/s10661-019-7193-x.
[4] V. Masindi, K.L. Muedi, Environmental contamination by heavy metals, in: H.E.-D. M. Saleh, R.F. Aglan (Eds.), Heavy Metals, InTech, 2018, https://doi.org/10.5772/intechopen.76082.
[5] D. Sud, G. Mahajan, M. Kaur, Agricultural waste material as potential adsorbent for sequestering heavy metal ions from aqueous solutions – a review, Bioresour. Technol. 99 (2008) 6017–6027, https://doi.org/10.1016/j.biortech.2007.11.064.
[6] N.T. Abdel-Ghani, M. Hefny, G.A.F. El-Chaghaby, Removal of lead from aqueous solution using low cost abundantly available adsorbents, Int. J. Environ. Sci. Technol. 4 (2007) 67–73, https://doi.org/10.1007/BF03325963.
[7] A.A. Alqadami, Z.A. ALOthman, M. Alsuhybani, M. Algamdi, Mu. Naushad, Excellent adsorptive performance of a new nanocomposite for removal of toxic Pb (II) from aqueous environment: adsorption mechanism and modeling analysis, Journal of Hazardous Materials. 389 (2020) 121896, https://doi.org/10.1016/j.jhazmat.2019.121896.

[8] T.K. Sen (Ed.), Air, Gas, and Water Pollution Control Using Industrial and Agricultural Solid Wastes Adsorbents, 1st ed., CRC Press, 2017 https://doi.org/10.1201/9781351228145.

[9] S. Afroze, T.K. Sen, A review on heavy metal ions and dye adsorption from water by agricultural solid waste adsorbents, Water Air Soil Pollut. 229 (2018) 225, https://doi.org/10.1007/s11270-018-3869-z.

[10] A. Demirbas, Heavy metal adsorption onto agro-based waste materials: a review, J. Hazard. Mater. 157 (2008) 220–229, https://doi.org/10.1016/j.jhazmat.2008.01.024.

[11] J. Mo, Q. Yang, N. Zhang, W. Zhang, Y. Zheng, Z. Zhang, A review on agro-industrial waste (AIW) derived adsorbents for water and wastewater treatment, J. Environ. Manag. 227 (2018) 395–405, https://doi.org/10.1016/j.jenvman.2018.08.069.

[12] Z.M. Şenol, Ü.D. Gül, R. Gurbanov, S. Şimşek, Optimization the removal of lead ions by fungi: explanation of the mycosorption mechanism, J. Environ. Chem. Eng. 9 (2021), 104760, https://doi.org/10.1016/j.jece.2020.104760.

[13] Z.M. Şenol, Ü.D. Gül, S. Şimşek, Assessment of Pb2+ removal capacity of lichen (Evernia prunastri): application of adsorption kinetic, isotherm models, and thermodynamics, Environ. Sci. Pollut. Res. 26 (2019) 27002–27013, https://doi.org/10.1007/s11356-019-05848-x.

[14] S. Jodeh, O. Hamed, A. Melhem, R. Salghi, D. Jodeh, K. Azzaoui, Y. Benmassaoud, K. Murtada, Magnetic nanocellulose from olive industry solid waste for the effective removal of methylene blue from wastewater, Environ. Sci. Pollut. Res. 25 (2018) 22060–22074, https://doi.org/10.1007/s11356-018-2107-y.

[15] R. Chakraborty, A. Asthana, A.K. Singh, B. Jain, A.B.H. Susan, Adsorption of heavy metal ions by various low-cost adsorbents: a review, Int. J. Environ. Anal. Chem. 102 (2022) 342–379, https://doi.org/10.1080/03067319.2020.1722811.

[16] O. Karnitz, L.V.A. Gurgel, J.C.P. de Melo, V.R. Botaro, T.M.S. Melo, R.P. de Freitas Gil, L.F. Gil, Adsorption of heavy metal ion from aqueous single metal solution by chemically modified sugarcane bagasse, Bioresour. Technol. 98 (2007) 1291–1297, https://doi.org/10.1016/j.biortech.2006.05.013.

[17] H.D. Doan, A. Lohi, V.B.H. Dang, T. Dang-Vu, Removal of Zn+2 and Ni+2 by adsorption in a fixed bed of wheat straw, Process Saf. Environ. Prot. 86 (2008) 259–267, https://doi.org/10.1016/j.psep.2008.04.004.

[18] F.N. Acar, Z. Eren, Removal of Cu(II) ions by activated poplar sawdust (Samsun Clone) from aqueous solutions, J. Hazard. Mater. 137 (2006) 909–914, https://doi.org/10.1016/j.jhazmat.2006.03.014.

[19] M.G.A. Vieira, A.F. de Almeida Neto, M.G.C. da Silva, C.N. Carneiro, A.A. Melo Filho, Adsorption of lead and copper ions from aqueous effluents on rice husk ash in a dynamic system, Braz. J. Chem. Eng. 31 (2014) 519–529, https://doi.org/10.1590/0104-6632.20140312s00002103.

[20] O.A. Hamed, S. Jodeh, N. Al-Hajj, E.M. Hamed, A. Abo-Obeid, Y. Fouad, Cellulose acetate from biomass waste of olive industry, J. Wood Sci. 61 (2015) 45–52, https://doi.org/10.1007/s10086-014-1442-y.

[21] H.-J. Hong, J.S. Lim, J.Y. Hwang, M. Kim, H.S. Jeong, M.S. Park, Carboxymethlyated cellulose nanofibrils(CMCNFs) embedded in polyurethane foam as a modular adsorbent of heavy metal ions, Carbohydr. Polym. 195 (2018) 136–142, https://doi.org/10.1016/j.carbpol.2018.04.081.

[22] M.S. Santos, E.S. Santos, M.J.S. Santos, W.N.L. dos Santos, A.S. Souza, D.S. de Jesus, C.F. das Virgens, M.S. Carvalho, N. Oleszczuk, M.G.R. Vale, B. Welz, S.L. C. Ferreira, V.A. Lemos, Application of polyurethane foam as a sorbent for trace metal pre-concentration — a review, Spectrochim. Acta B At. Spectrosc. 62 (2007) 4–12, https://doi.org/10.1016/j.sab.2006.12.006.

[23] A. Anthemidis, G. Zachariadis, J. Stratis, On-line preconcentration and determination of copper, lead and chromium(VI) using unloaded polyurethane foam packed column by flame atomic absorption spectrometry in natural waters and biological samples, Talanta 58 (2002) 831–840, https://doi.org/10.1016/S0039-9140(02)00373-9.

[24] S.M. Abdel Azeem, S.M. Mohamed Attaf, M.F. El-Shahat, Acetylacetone phenylhydrazone functionalized polyurethane foam: determination of copper, zinc and manganese in environmental samples and pharmaceutics using flame atomic absorption spectrometry, React. Funct. Polym. 73 (2013) 182–191, https://doi.org/10.1016/j.reactfunctpolym.2012.10.007.

[25] Sami Mohammed Abdel Azeem Abdel Salam, Chemically Modified Polyurethane Foam for Pre-concentration and separation of inorganic and organic species, 2008.

[26] E. Dacewicz, J. Grzybowska-Pietras, Polyurethane foams for domestic sewage treatment, Materials 14 (2021) 933, https://doi.org/10.3390/ma14040933.

[27] S. Kumari, G.S. Chauhan, J. Ahn, Novel cellulose nanowhiskers-based polyurethane foam for rapid and persistent removal of methylene blue from its aqueous solutions, Chem. Eng. J. 304 (2016) 728–736, https://doi.org/10.1016/j.cej.2016.07.008.

[28] Y. Zhao, D.G. Truhlar, The M06 suite of density functionals for main group thermochemistry, thermochemical kinetics, noncovalent interactions, excited states, and transition elements: two new functionals and systematic testing of four M06-class functionals and 12 other functionals, Theor Chem Account. 120 (2008) 215–241, https://doi.org/10.1007/s00214-007-0310-x.

[29] M.Ben Hadj Ayed, T. Osmani, N. Issaoui, A. Berisha, B. Oujia, H. Ghalla, Structures and relative stabilities of Na+Nen (n = 1–16) clusters via pairwise and DFT calculations, Theor Chem Acc. 138 (2019) 84, https://doi.org/10.1007/s00214-019-2476-4.

[30] N. Mardirossian, M. Head-Gordon, Thirty years of density functional theory in computational chemistry: an overview and extensive assessment of 200 density functionals, Mol. Phys. 115 (2017) 2315–2372, https://doi.org/10.1080/00268976.2017.1333644.

[31] A. Berisha, Interactions between the aryldiazonium cations and graphene oxide: a DFT study, J. Chem. 2019 (2019) 1–5, https://doi.org/10.1155/2019/5126071.

[32] A. Klamt, The COSMO and COSMO-RS solvation models, WIREs Comput. Mol. Sci. 1 (2011) 699–709, https://doi.org/10.1002/wcms.56.

[33] S.J.H.M. Jessima, SS, A. Berisha, A. Oral, S.S. Srikandan, Corrosion mitigation performance of disodium EDTA functionalized chitosan biomacromolecule - experimental and theoretical approach, International Journal of Biological Macromolecules 178 (2021) 477–491, https://doi.org/10.1016/j.ijbiomac.2021.02.166.

[34] M. Rbaa, P. Dohare, A. Berisha, O. Dagdag, L. Lakhrissi, M. Galai, B. Lakhrissi, M. E. Touhami, I. Warad, A. Zarrouk, New epoxy sugar based glucose derivatives as eco friendly corrosion inhibitors for the carbon steel in 1.0 M HCl: experimental and theoretical investigations, J. Alloys Compd. 833 (2020), 154949, https://doi.org/10.1016/j.jallcom.2020.154949.

[35] R. Hsissou, O. Dagdag, S. Abbout, F. Benhiba, M. Berradi, M. El Bouchti, A. Berisha, N. Hajjaji, A. Elharfi, Novel derivative epoxy resin TGETET as a corrosion inhibition of E24 carbon steel in 1.0 M HCl solution. Experimental and computational (DFT and MD simulations) methods, J. Mol. Liq. 284 (2019) 182–192, https://doi.org/10.1016/j.molliq.2019.03.180.

[36] A. Berisha, Experimental, Monte Carlo and Molecular dynamic study on corrosion inhibition of mild steel by pyridine derivatives in aqueous perchloric acid, Electrochem. 1 (2020) 188–199, https://doi.org/10.3390/electrochem1020013.

[37] O. Amrhar, A. Berisha, L. El Gana, H. Nassali, M.S. Elyoubi, Removal of methylene blue dye by adsorption onto natural muscovite clay: experimental, theoretical and computational investigation, Int. J. Environ. Anal. Chem. (2021) 1–26, https://doi.org/10.1080/03067319.2021.1897119.

[38] O. Hamed, M. Qaisi, I. Abushqair, A. Berisha, O. Dagdag, A. Janem, K. Azzaoui, R. Al-Kerm, R. Al-Kerm, B. Hammouti, Cellulose powder functionalized with phenyl biguanide: synthesis, cross-linking, metal adsorption, and molecular docking, BioRes. 16 (2021) 7263–7282, https://doi.org/10.15376/biores.16.4.7263-7282.

[39] B. Khalaf, O. Hamed, S. Jodeh, R. Bol, G. Hanbali, Z. Safi, O. Dagdag, A. Berisha, S. Samhan, Cellulose-based hectocycle nanopolymers: synthesis, molecular docking and adsorption of difenoconazole from aqueous medium, IJMS 22 (2021) 6090, https://doi.org/10.3390/ijms22116090.

[40] H. Babas, M. Khachani, I. Warad, S. Ajebli, A. Guessous, A. Guenbour, Z. Safi, A. Berisha, A. Bellaouchou, Z. Abdelkader, G. Kaichouh, Sofosbuvir adsorption onto activated carbon derived from argan shell residue: optimization, kinetic, thermodynamic and theoretical approaches, J. Mol. Liq. 356 (2022), 119019, https://doi.org/10.1016/j.molliq.2022.119019.

[41] N. Hasani, T. Selimi, A. Mele, V. Thaçi, J. Halili, A. Berisha, M. Sadiku, Theoretical, equilibrium, kinetics and thermodynamic investigations of methylene blue adsorption onto lignite coal, Molecules 27 (2022) 1856, https://doi.org/10.3390/molecules27061856.

[42] O. Hamed, B.A. Lail, A. Deghles, B. Qasem, K. Azzaoui, A.A. Obied, M. Algarra, S. Jodeh, Synthesis of a cross-linked cellulose-based amine polymer and its application in wastewater purification, Environ. Sci. Pollut. Res. 26 (2019) 28080–28091, https://doi.org/10.1007/s11356-019-06001-4.

[43] J.M. Lázaro Martínez, P.N. Romasanta, A.K. Chattah, G.Y. Buldain, NMR characterization of hydrate and aldehyde forms of Imidazole-2-carboxaldehyde and derivatives, J. Org. Chem. 75 (2010) 3208–3213, https://doi.org/10.1021/jo902588s.

[44] M. Iqhrammullah, M. Marlina, H.P.S.A. Khalil, K.H. Kurniawan, H. Suyanto, R. Hedwig, I. Karnadi, N.G. Olaiya, C.K. Abdullah, S.N. Abdulmadjid, Characterization and performance evaluation of cellulose acetate-polyurethane film for Lead II ion removal, Polymers 12 (2020) 1317, https://doi.org/10.3390/polym12061317.

[45] U.-J. Kim, Y.R. Lee, T.H. Kang, J.W. Choi, S. Kimura, M. Wada, Protein adsorption of dialdehyde cellulose-crosslinked chitosan with high amino group contents, Carbohydr. Polym. 163 (2017) 34–42, https://doi.org/10.1016/j.carbpol.2017.01.052.

[46] J.X. Lin, S.L. Zhan, M.H. Fang, X.Q. Qian, H. Yang, Adsorption of basic dye from aqueous solution onto fly ash, J. Environ. Manag. 87 (2008) 193–200, https://doi.org/10.1016/j.jenvman.2007.01.001.

[47] R. Pino-Rios, E. Chigo-Anota, E. Shakerzadeh, G. Cárdenas-Jirón, B12N12 cluster as a collector of noble gases: a quantum chemical study, Physica E 115 (2020), 113697, https://doi.org/10.1016/j.physe.2019.113697.

[48] G. Mahmoudi, M. Abedi, S.E. Lawrence, E. Zangrando, M.G. Babashkina, A. Klein, A. Frontera, D.A. Safin, Tetrel bonding and other non-covalent interactions assisted supramolecular aggregation in a new Pb(II) complex of an isonicotinohydrazide, Molecules 25 (2020) 4056, https://doi.org/10.3390/molecules25184056.

[49] M. Kowalik, J. Masternak, J. Brzeski, M. Daszkiewicz, B. Barszcz, Effect of a lone electron pair and tetrel interactions on the structure of Pb(II) CPs constructed from pyrimidine carboxylates and auxiliary inorganic ions, Polyhedron 219 (2022), 115818, https://doi.org/10.1016/j.poly.2022.115818.

[50] A. Moncomble, J.-P. Cornard, M. Meyer, A quantum chemistry evaluation of the stereochemical activity of the lone pair in PbII complexes with sequestering ligands, J. Mol. Model. 23 (2017) 24, https://doi.org/10.1007/s00894-016-3190-y.

[51] R. Hsissou, B. Benzidia, M. Rehioui, M. Berradi, A. Berisha, M. Assouag, N. Hajjaji, A. Elharfi, Anticorrosive property of hexafunctional epoxy polymer HGTMDAE for E24 carbon steel corrosion in 1.0 M HCl: gravimetric, electrochemical, surface morphology and molecular dynamic simulations, Polym. Bull. 77 (2020) 3577–3601, https://doi.org/10.1007/s00289-019-02934-5.

[52] S. Abbout, M. Zouarhi, D. Chebabe, M. Damej, A. Berisha, N. Hajjaji, Galactomannan as a new bio-sourced corrosion inhibitor for iron in acidic media, Heliyon 6 (2020), e03574, https://doi.org/10.1016/j.heliyon.2020.e03574.

[53] O. Dagdag, R. Hsissou, A. Berisha, H. Erramli, O. Hamed, S. Jodeh, A. El Harfi, Polymeric-based epoxy cured with a polyaminoamide as an anticorrosive coating for aluminum 2024–T3 surface: experimental studies supported by computational modeling, J Bio Tribo Corros. 5 (2019) 58, https://doi.org/10.1007/s40735-019-0251-7.

[54] O. Dagdag, R. Hsissou, A. El Harfi, A. Berisha, Z. Safi, C. Verma, E.E. Ebenso, M. Ebn Touhami, M. El Gouri, Fabrication of polymer based epoxy resin as effective anti-corrosive coating for steel: computational modeling reinforced experimental studies, Surf. Interfaces 18 (2020), 100454, https://doi.org/10.1016/j.surfin.2020.100454.

[55] V. Mehmeti, M. Sadiku, A comprehensive DFT investigation of the adsorption of polycyclic aromatic hydrocarbons onto graphene, Computation. 10 (2022) 68, https://doi.org/10.3390/computation10050068.

[56] M. Sadiku, T. Selimi, A. Berisha, A. Maloku, V. Mehmeti, V. Thaçi, N. Hasani, Removal of methyl violet from aqueous solution by adsorption onto halloysite nanoclay: experiment and theory, Toxics. 10 (2022) 445, https://doi.org/10.3390/toxics10080445.

[57] S. Ajebli, G. Kaichouh, M. Khachani, H. Babas, M. El Karbane, I. Warad, Z.S. Safi, A. Berisha, V. Mehmeti, A. Guenbour, A. Bellaouchou, A. Zarrouk, The adsorption of tenofovir in aqueous solution on activated carbon produced from maize cobs: insights from experimental, molecular dynamics simulation, and DFT calculations, Chem. Phys. Lett. 801 (2022), 139676, https://doi.org/10.1016/j.cplett.2022.139676.

[58] N. Nairat, O. Hamed, A. Berisha, S. Jodeh, M. Algarra, K. Azzaoui, O. Dagdag, S. Samhan, Cellulose polymers with β-amino ester pendant group: design, synthesis, molecular docking and application in adsorption of toxic metals from wastewater, BMC Chem. 16 (2022) 43, https://doi.org/10.1186/s13065-022-00837-7.

[59] M. El Faydy, H. About, I. Warad, Y. Kerroum, A. Berisha, F. Podvorica, F. Bentiss, G. Kaichouh, B. Lakhrissi, A. Zarrouk, Insight into the corrosion inhibition of new bis-quinolin-8-ols derivatives as highly efficient inhibitors for C35E steel in 0.5 M H2SO4, J. Mol. Liq. 342 (2021), 117333, https://doi.org/10.1016/j.molliq.2021.117333.

[60] Abdu Molhi, Rachid Hsissou, Mohamed Damej, Avni Berisha, A. Veprim Thaçi, M. Benmessaoud Belafhaili, Najoua Labjar, Souad El Hajjaji, Performance of two epoxy compounds against corrosion of C38 steel in 1 M HCl: electrochemical, thermodynamic and theoretical assessment, Int. J. Corros. Scale Inhib. 10 (2021), https://doi.org/10.17675/2305-6894-2021-10-2-21.